J Mater Sci (2012) 47:465–472
DOI 10.1007/s10853-011-5821-0

Photocatalytic activity of magnetically separable La-doped $TiO_2/CoFe_2O_4$ nanofibers prepared by two-spinneret electrospinning

Xiu-Yan Li · Jiao-Na Wang · Lian-Lian Zhang · Cong-Ju Li

Received: 1 June 2011 / Accepted: 25 July 2011 / Published online: 4 August 2011

Abstract A novel magnetically separable composite photocatalyst—⟨La-doped TiO_2⟩/$CoFe_2O_4$ nanofiber—was prepared by a two-spinneret electrospinning method combined with sol–gel method. The nanofibers were characterized by X-ray diffraction (XRD), scanning electron microscopy (SEM), transmission electron microscope (TEM), Energy dispersive X-ray spectroscopy (EDS), X-ray photoelectron spectroscopy (XPS), and vibrating sample magnetometer (VSM). It was shown that the diameter of ⟨1.0% La-doped TiO_2⟩/$CoFe_2O_4$ nanofibers was 100–150 nm after calcination at 600 °C for 2 h. EDS and XPS measurements on the photocatalytic material indicated the existence of La^{3+} oxidation states in ⟨1.0% La-doped TiO_2⟩/$CoFe_2O_4$ nanofibers. The photocatalytic activity of as-prepared nanofibers was evaluated using methylene blue (MB) as a model organic compound and the result revealed that the ⟨1.0% La-doped TiO_2⟩/$CoFe_2O_4$ nanofibers have an efficient photocatalytic property, and the degradation rate of MB could reach 93% in 150 min. Moreover, the magnetic property of the nanofibers has also been characterized, and the nanofibers show a good magnetic response, which indicates that the possibility of the magnetic nanofibers' potential recycling property.

X.-Y. Li · J.-N. Wang · L.-L. Zhang · C.-J. Li (✉)
College of Material Science and Engineering, Beijing Institute of Fashion Technology, Beijing 100029, China
e-mail: congjuli@gmail.com

J.-N. Wang · L.-L. Zhang · C.-J. Li
Beijing Key Laboratory of Clothing Materials R&D and Assessment, Beijing 100029, China

Introduction

Titanium dioxide (TiO_2) semiconductor photocatalysts have attracted much attention in heterogeneous photocatalysis and in advanced oxidation processes because of its strong oxidizing power, nontoxicity, thermal and chemical stability, low-cost, and insolubility [1–4]. It is proved that by UV light irradiation of TiO_2, electrons in the valence band will jump to the conduction band, and an electron–hole pair (e^-/h^+) is generated [5, 6]. The e^-/h^+ will act as strong oxidizing agents that can easily attack any organic molecules adsorbed on, or those located close to the surface of the catalyst, thus, it could achieve rapid and complete degradation to inorganic products [7]. However, Anatase TiO_2 with a band gap of 3.2 eV can be photoexcited under irradiation of UV light ($\lambda < 387$ nm), which is only about 2–5% of sunlight [8, 9].

To enhance the efficiency of TiO_2 photocatalytic activity, several strategies have been involved, including surface sensitization [10–12], metal ion doping [13–15], non-metal ion doping [16, 17], and noble metal loading [18, 19]. Among different modification methods, doping with rare earth ions is an effective method [20]. Lanthanide-ions are known for their ability to form complexes with various Lewis bases (e.g., acids, amines, alcohols, aldehydes, thiols, etc.) in the interaction of these functional groups with *f*-orbital of the lanthanides [6, 21]. The incorporation of La^{3+} into a TiO_2 matrix could provide a means to concentrate the organic pollutant at the semiconductor surface [22]. Cao et al. [8] demonstrated that the high specific surface area resulting from La doping could enhance the ability of MB to be adsorbed onto TiO_2, which also caused the enhancement of adsorption capacity of TiO_2. Ranjit et al. [15] reported that doping of TiO_2 with rare earth ions could lead to red shift of absorption edge,

which was one of the important ways to improve the photocatalytic activity of TiO_2. In addition, it could improve the photochemical properties by increasing the separation of e^-/h^+ under UV light [23].

Meanwhile, another main drawback of TiO_2 is that the separation of nanosized photocatalysts from wastewater and their recycling are difficult and uneconomical. Therefore, a magnetic photocatalyst is developed to solve this problem. The magnetic photocatalyst can allow easy separation by applying an external magnetic field, without the need for further downstream treatment processes [24, 25].

Herein, we prepared ⟨La-doped TiO_2⟩/$CoFe_2O_4$ photocatalytic nanofibers by a novel two-spinneret electrospinning technique [26] and sol–gel method, which offered considerably higher photocatalytic efficiency, and the nanofibers were easy to be separated from the treated water under the application of an external magnetic field.

Experimental

Materials

Cobalt(II) nitrate hexahydrate [$Co(NO_3)_2{\cdot}6H_2O$, 99.0%, A.R. Tientsin Fuchen Chemical Reagents Co.] and Ferric(III) nitrate nonahydrate [$Fe(NO_3)_3{\cdot}9H_2O$, 98.5%, A.R. Tientsin Fuchen Chemical Reagents Co.) were used as precursors. Citric acid monohydrate ($C_6H_8O_7{\cdot}H_2O$, 99.5%, Tientsin Fuchen Chemical Reagents Co.) was used as a chelating agent. Ammonia water ($NH_3{\cdot}H_2O$, 25%, A.R. Tientsin Fuchen Chemical Reagents Co.) was used to adjust pH of the solution. Poly(vinyl pyrrolidone) (PVP, $M_r = 10{,}000$, A.R. Tientsin Fuchen Chemical Reagents Co.), Acetic acid (CH_3COOH, HAc, 99.5%, A.R. Beijing Chemical Works), and Anhydrous ethanol (CH_3CH_2OH, EtOH, A.R. Beijing Chemical Works) were used as a spinning aid. For the preparation of the TiO_2 precursor, Tetrabutyl titanate ($Ti[O(CH_2)_3CH_3]_4$, A.R. Beijing Chemical Works) was chosen as Ti resource. Lanthanum(III) acetate ($La(Ac)_3$, 0.5 mol L^{-1}) was dropped into the TiO_2 precursor solution. Methylene blue (MB) was obtained from Beijing Zhongxiyuanda Corporation to act as an organic pollutant in waste water. Degussa P25 (with 80% anatase and 20% rutile) was produced by Degussa AG Company in Germany.

Synthesis of ⟨La-doped TiO_2⟩/$CoFe_2O_4$ photocatalysts

Preparation of $CoFe_2O_4$ sol

The precursor solution for $CoFe_2O_4$ was prepared by dissolving 1.00 g cobalt(II) nitrate hexahydrate, 2.78 g Ferric(III) nitrate nonahydrate, and 1.98 g citric acid monohydrate in 30 mL deionized water. The molar ratio between cobalt and iron was 1:2. Adjust the pH value to 5–6 utilize the pH analyzer under the magnetic stirring. Subsequently, the mixture was heated at 60 °C with constant stirring to allow evaporation to form wet gel. A metal precursor/PVP solution was prepared by dissolving 3 mL gel into 22 wt% PVP/HAc solution and stirred for 12 h.

Preparation of La-doped TiO_2 precursor

La-doped TiO_2 precursor was prepared by the following procedures: An aid spun agent was made by adding 4 g PVP to 15 mL ethanol in a small quartz conical flask. Then, the solution was sonicated for 30 min to allow PVP to disperse well. The precursor solution was made in another conical flask by stirring 1 mL $Ti[O(CH_2)_3CH_3]_4$ and 1 mL glacial acetic acid. The precursor solution was poured into the PVP/EtOH solution slowly and stirred for 2 h. Then, 0.05 mL $La(Ac)_3$ was added slowly into the above mixed solution. After being stirred for 2 h, La-doped TiO_2 precursor was obtained. The sample had a nominal mass ratio (La/Ti) of 1.0%, which was named as 1.0% La-doped TiO_2 in this study. The other La-doped TiO_2 samples containing different rare earth ion contents were prepared using the same procedure with different contents of $La(Ac)_3$, and the obtained catalysts were named as 1.5% La-doped TiO_2 and 2.0% La-doped TiO_2, respectively.

Preparation of ⟨La-doped TiO_2⟩/$CoFe_2O_4$ nanofibers

The electrospinning process was carried out using a self-made apparatus. Figure 1 shows the scheme of the hybrid electrospinning apparatus to fabricate ⟨La-doped TiO_2⟩/$CoFe_2O_4$ nanofibers. The spinneret containing the La-doped TiO_2 precursor solution had an inner diameter of about 1.0 mm, the other was 0.5 mm. After electrospinning, these precursor nanofibers were dried in air atmosphere at 60 °C for 12 h, and then calcined at different

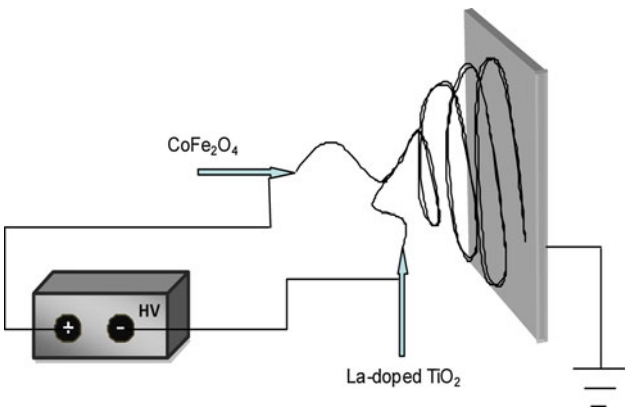

Fig. 1 Scheme of the hybrid electrospinning process

temperatures (550, 600, and 650 °C) with the heating rate of 150 °C h^{-1} to obtain the composite nanofibers.

Characterization of ⟨La-doped TiO_2⟩/$CoFe_2O_4$ nanofibers

The ⟨La-doped TiO_2⟩/$CoFe_2O_4$ composite photocatalysts were examined by X-ray diffraction (XRD, 40 kV, 200 mA, D/MAX-IIIA, Rigaku, Tokyo, Japan) using a CuKα radiation with $\lambda = 0.154056$ nm. Scanning electron microscopy (SEM, JSM-6360LV, Tokyo, Japan) and transmission electron microscope (TEM, Tecnai G^2 20 S-TWIN) were employed to investigate their morphology. Energy dispersive X-ray spectroscopy (EDS, accessory in SEM) and X-ray photoelectron spectroscopy (XPS, ESCALAB 250) were used for composition analysis. The vibrating sample magnetometer (VSM, Lake shore 7410, Lake Shore Cryotronics) was utilized to examine the magnetic properties.

Evaluation of photocatalytic property

The photocatalytic activity of ⟨La-doped TiO_2⟩/$CoFe_2O_4$ nanofibers was measured by the photodegradation of MB aqueous solution, and Fig. 2 shows the schematic representation of the photoreactor [27]. The dosage of photocatalyst was constant in our experiments (30 mg samples in 400 mL solution) for an easy comparison. The initial concentration of MB solution was 25 mg/L. In photocatalytic experiments, an aqueous solution of MB containing the photocatalyst was stirred in the dark to permit the adsorption/desorption equilibrium until the concentration of MB solution was constant. After a definite irradiation time (30 min), 3 mL of dispersion was centrifuged to separate the photocatalyst. The supernatant solution was analyzed by an UV–Vis spectrophotometer (Beijing Purkinje General Instrument Co., Ltd) at the wavelength of 666 nm.

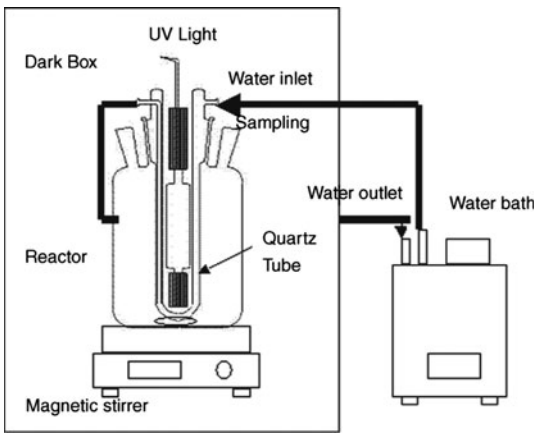

Fig. 2 Schematic representation of the photoreactor

Results and discussions

X-ray diffraction analysis

Figure 3 shows XRD patterns of ⟨1.5% La-doped TiO_2⟩/$CoFe_2O_4$ calcined from 550 to 650 °C for 2 h. There are a sharp and strong peak of spinel $CoFe_2O_4$ ($2\theta = 30.1°$, 35.4°, 43.0°, 53.4°, 74.0°), a clear peak of anatase ($2\theta = 25.2°$, 37.8°, 48.0°, 54.2°, 62.6°), and small amounts of the rutile ($2\theta = 27.4°$, 36.0°, 56.7°) in the XRD patterns. The content of anatase TiO_2 in each sample can be calculated by the following equation: $\omega(A) = 100\%/(1 + 1.265I_R/I_A)$, where I_A and I_R are the highest peak intensity of anatase phase (101) and the rutile phase (110), respectively [28]. The results are listed in Table 1. The optimal calcination temperature was 600 °C, with anatase to rutile ratio of 84:16. For most photocatalytic reaction systems, it is generally accepted that anatase demonstrates a higher activity than rutile [29], and a mixture of anatase and rutile has higher activity than pure anatase or rutile [30]. In addition, Degussa P25 titania catalyst, which is also a mixture consisting of 80% anatase and 20% rutile, has been extensively used as a photocatalyst [31]. These results show that introducing some rutile may enhance the photocatalytic properties of anatase. Fig. 3 also shows that

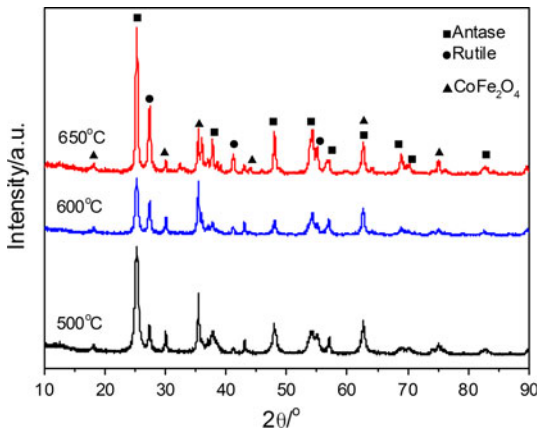

Fig. 3 XRD patterns of ⟨1.5% La-doped TiO_2⟩/$CoFe_2O_4$ nanofibers sintered at different temperatures for 2 h

Table 1 The effect of calcination temperature on the content of anatase TiO_2

Sample	Calcination temperatures/°C	Relative phase content/%	
		Anatase	Rutile
⟨1.5% La-doped TiO_2⟩/$CoFe_2O_4$	550	62	38
	600	84	16
	650	73	27

when the calcination temperature increases from 550 to 650 °C, the peak intensities of anatase increase at first and then decrease, indicating that the best crystallinity is obtained at 600 °C.

Figure 4 shows the XRD patterns of ⟨La-doped TiO_2⟩/$CoFe_2O_4$ nanofibers with different contents of La (1.0, 1.5, and 2.0%), which were calcined at 600 °C for 2 h. According to the XRD patterns, the composite nanofibers have formed a mixed phase of spinel $CoFe_2O_4$ and anatase/rutile TiO_2. The phase structures are hardly affected by La doping. In addition to this, the La phase cannot be observed in the patterns. The main reasons for this are as follows: (1) the lower amount of doped La is thoroughly dispersed within the Ti–O–Ti network during the dissolving process; and (2) the ionic radius of La^{3+} (1.06 Å) is larger than Ti^{4+} (0.605 Å) [32, 33], which inhibit the ion from embedding into the lattice of TiO_2.

SEM/TEM analysis

Figure 5 shows the morphological and structural details of the ⟨1.0% La-doped TiO_2⟩/$CoFe_2O_4$ nanofibers obtained after heating for 2 h. Figure 5a shows the SEM micrograph of ⟨1.0% La-doped TiO_2⟩/$CoFe_2O_4$ nanofibers. The nanofibers appear with an agglomerate phenomenon, which is probably attributed to that the solvent cannot evaporate entirely in the calcination process. And the diameter of the nanofibers is 100–150 nm. The TEM image (Fig. 5b) also shows that the diameter of the obtained composite nanofiber is about 100 nm. And the corresponding SAED pattern of the nanofiber presents spotty rings which can be indexed to the polycrystalline structure of spinel $CoFe_2O_4$ and anatase/rutile-phase TiO_2.

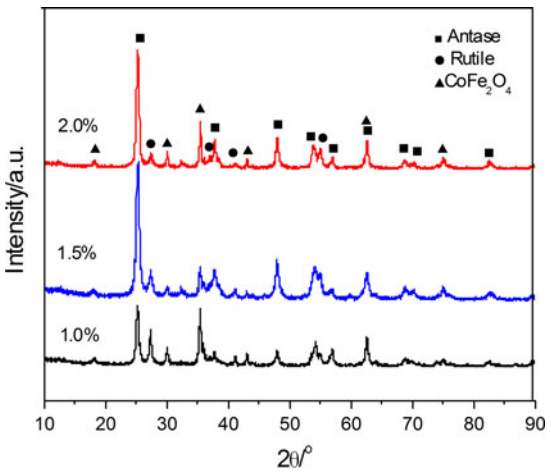

Fig. 4 XRD patterns of ⟨La-doped TiO_2⟩/$CoFe_2O_4$ nanofibers obtained at 600 °C for 2 h with different amounts of La

EDS analysis

Figure 6 shows the EDS spectra of ⟨1.0% La-doped TiO_2⟩/$CoFe_2O_4$ nanofibers. It should be mentioned that in our experiment, it can be concluded from the EDS results that the nanofibers consisted of Ti, O, Fe, Co, and La elements. It testifies that La is indeed doped in the nanofibers. Meanwhile, the Au element observed in the EDS is associated with the coating (gold) used to avoid charging of the sample.

XPS analysis

The elemental composition and chemical state of ⟨1.0% La-doped TiO_2⟩/$CoFe_2O_4$ nanofibers were characterized using XPS (Fig. 7). It can be seen that the surface of ⟨1.0% La-doped TiO_2⟩/$CoFe_2O_4$ nanofibers is composed of Ti, O, Co, Fe, and La elements, which is consistent with the result of EDS. Meanwhile, Fig. 7f shows the XPS pattern of La 3*d*, and the multiple peaks around 830–840 and 850–860 eV indicated the existence of La^{3+} oxidation states in ⟨1.0% La-doped TiO_2⟩/$CoFe_2O_4$ nanofibers. However, the diffraction peaks of La^{3+} were not observed from the XRD pattern in Figs. 3 and 4, probably indicating that the La^{3+} compound had a very low content. Therefore, EDS and XPS measurements on the photocatalytic material reveal the presence and oxidation state of the Lanthanum ions.

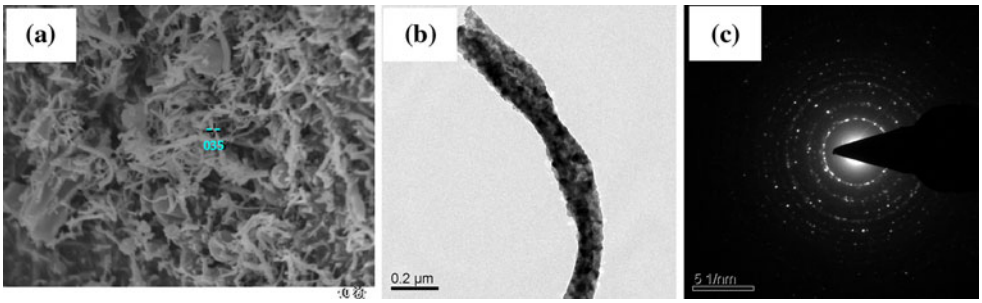

Fig. 5 **a** SEM and **b** TEM images of as-synthesized ⟨1.0% La-doped TiO_2⟩/$CoFe_2O_4$ nanofibers **c** corresponding SAED pattern from the region in (**b**)

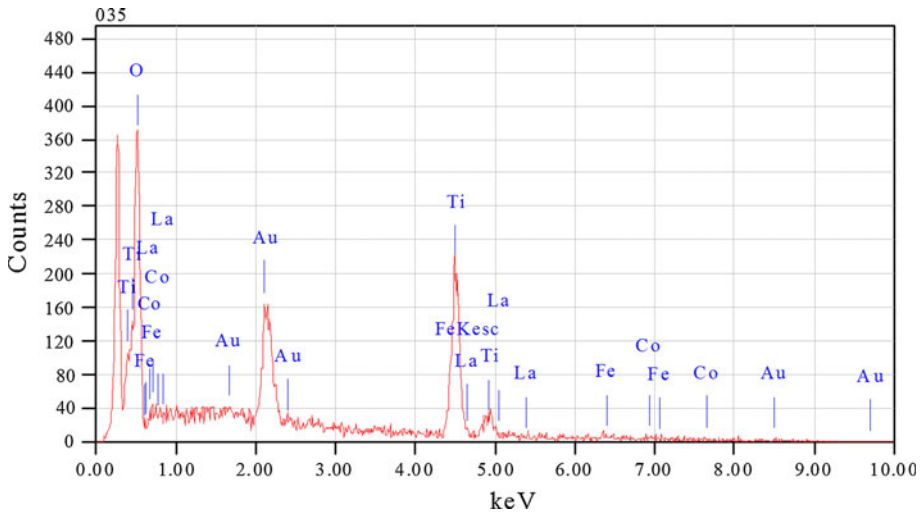

Fig. 6 EDS spectra of ⟨1.0% La-doped TiO_2⟩/$CoFe_2O_4$ nanofibers

UV–Vis spectroscopic analysis

Figure 8 presents the UV–Vis absorption spectra of different samples. Degussa P25 titania as a standard photocatalyst was also applied in the photocatalytic experiments in order to compare photoactivity of the as-prepared composite fibers. From the spectra, we can see that all of the samples have absorption in the whole ultraviolet light and visible light region. Moreover, the intensity of this absorption is found to increase with decreasing of La doping content in the whole region (190–800 nm). The result indicates that their photocatalytic activity gradually increases as the content of La is on decrease.

Photocatalytic experiments of ⟨La-doped TiO_2⟩/$CoFe_2O_4$ nanofibers

Photocatalytic properties of composite nanofibers with different amounts of La

The photocatalytic properties of the prepared ⟨La-doped TiO_2⟩/$CoFe_2O_4$ nanofibers with different contents of La (1.0, 1.5, and 2.0%) for photodegradation of MB under UV irradiation are shown in Fig. 9. The degradation rate of MB monotonically decreases from 93 to 85% as the content of La rises, which is consistent with the UV–Vis reflectance spectra in Fig. 8. Xu et al. [34] reported that there existed an optimum doping content of rare earth ions in TiO_2 particles for the most efficient separation of photoinduced electron–hole pairs. When La^{3+} adulterant proportion (mass ratio) is high, the space charge region becomes very narrow, and the depth of penetration of light into TiO_2 greatly exceeds the space charge layer. Therefore, the recombination of the photoinduced electron–hole pairs becomes easier. Consequently, the photocatalytic activity begins to decrease [35, 36].

Furthermore, the experimental results obtained from Fig. 9 show that all of the samples have lower photocatalytic activities than P25, which is known as the best photocatalyst commercially available. But after irradiation for 150 min the photoactivities of ⟨1.0% La-doped TiO_2⟩/$CoFe_2O_4$ is near to that of P25.

Photocatalytic activity of composite nanofibers at different calcination temperatures

Figure 10 shows the photocatalytic activity of the prepared ⟨1.0% La-doped TiO_2⟩/$CoFe_2O_4$ at different calcination temperatures. The sample calcined at 600 °C displays the highest degradation of MB under UV irradiation, and 93% of MB in solution is removed after 150 min reaction. The results clearly demonstrate that the degradation rate increases with the increase of calcination temperature of ⟨1.0% La-doped TiO_2⟩/$CoFe_2O_4$ up to 600 °C, but further increasing calcination temperature (up to 650 °C) leads to an obvious decrease in degradation. This feature indicates that the calcination temperature has an important influence on photoactivity of ⟨1.0% La-doped TiO_2⟩/$CoFe_2O_4$ nanofibers.

Effect of initial concentration of MB

Figure 11 shows the results of the photocatalytic degradation of MB under UV light irradiation, using 30 mg of ⟨1.0% La-doped TiO_2⟩/$CoFe_2O_4$ nanofibers as a photocatalyst. And the results show that the degradation rate decreases with the MB concentration increasing, and this result is in accordance with the reported literature [37]. It could be due to the fact that higher concentration of MB means that the capacity of light penetrating solution decreases, and the photon number participating in photocatalysis also decreases. So with the MB concentration

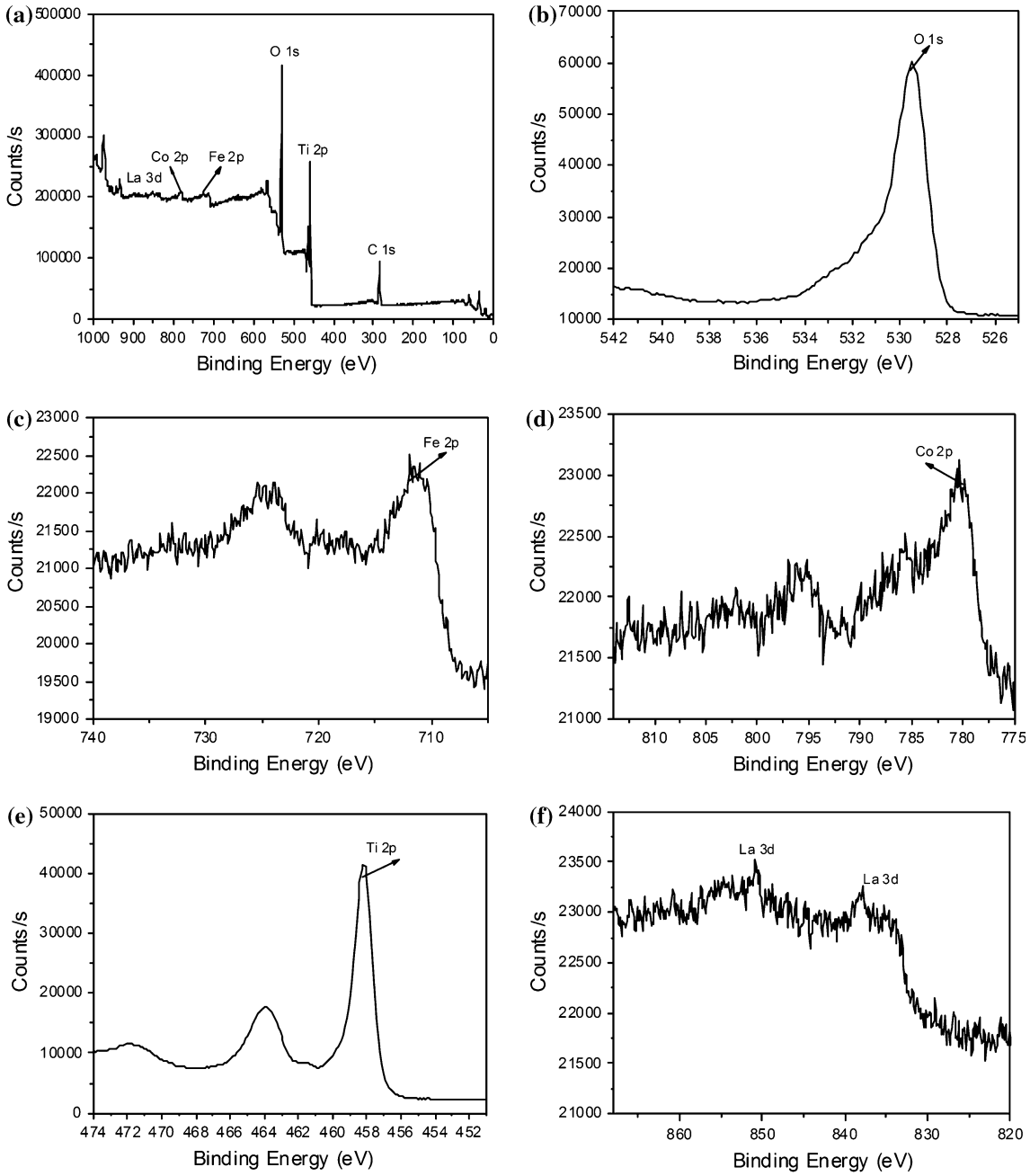

Fig. 7 XPS patterns of ⟨1.0% La-doped TiO_2⟩/$CoFe_2O_4$ nanofibers. **a** The whole survey, **b** high-resolution spectra of O 1*s*, **c** high-resolution spectra of Fe 2*p*, **d** high-resolution spectra of Co 2*p*, **e** high-resolution spectra of Ti 2*p*, **f** high-resolution spectra of La 3*d*

increasing, the photodegradation ratio of MB decreases [38].

Magnetic properties of composite nanofibers

Figure 12 shows the magnetic properties of ⟨1.0% La-doped TiO_2⟩/$CoFe_2O_4$ and pure $CoFe_2O_4$ nanofibers. Both of them show typical ferromagnetic hysteresis. The saturation magnetization (M_s) of $CoFe_2O_4$ and ⟨1.0% La-doped TiO_2⟩/$CoFe_2O_4$ nanofibers are found to be 49.007 and 8.8880 A m^2 kg^{-1}, respectively. The differences of M_s between the nanofibers are based on the weight of $CoFe_2O_4$ in the composite nanofibers. And the coercivity (H_c) of ⟨1.0% La-doped TiO_2⟩/$CoFe_2O_4$ nanofibers does not show any change. Coercivity represents the magnetic properties of material, so it is believed that these ⟨1.0% La-doped TiO_2⟩/$CoFe_2O_4$ nanofibers will allow the use of a magnet or a magnetic field for an easy solid/liquid separation.

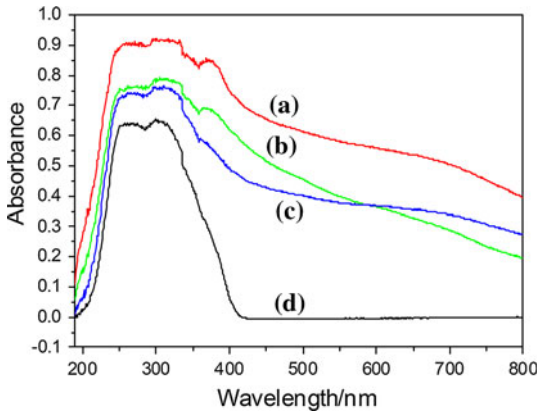

Fig. 8 UV–Vis absorption spectra of different samples. *a* 1.0%, *b* 1.5%, *c* ⟨2.0% La-dopedTiO_2⟩/$CoFe_2O_4$, and *d* P25

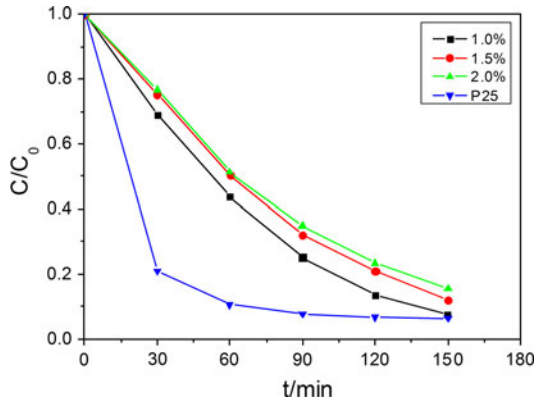

Fig. 9 Photocatalytic activity of ⟨La-doped TiO_2⟩/$CoFe_2O_4$ nanofibers obtained at 600 °C for 2 h with different amounts of La and P25

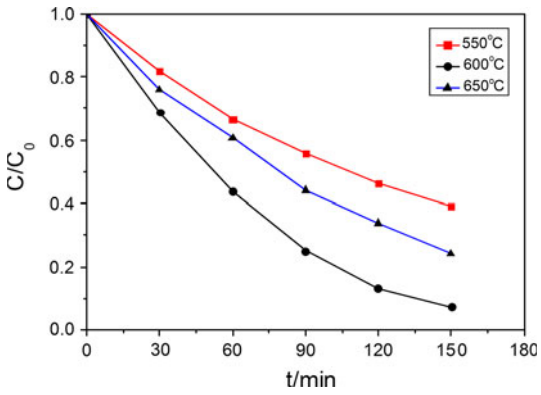

Fig. 10 Photocatalytic activity of the prepared ⟨1.0% La-doped TiO_2⟩/$CoFe_2O_4$ nanofibers at different calcination temperatures

Conclusions

A magnetic-semiconductor photocatalyst made of TiO_2/$CoFe_2O_4$ composite fibers doped with La has been prepared via sol–gel and electrospinning method. The nanofibers have proved to be an excellent photocatalyst, and the photodegradation ratio of MB by ⟨1.0% La-doped TiO_2⟩/$CoFe_2O_4$ composite nanofibers was up to 93%. The coercivity of the nanofibers is similar to that of $CoFe_2O_4$ nanofiber, which indicates the possibility of its potential recycling property. So it is believed that these nanofibers may serve as a new generation of high efficiency photocatalyst, and can be recycled to avoid secondly pollution.

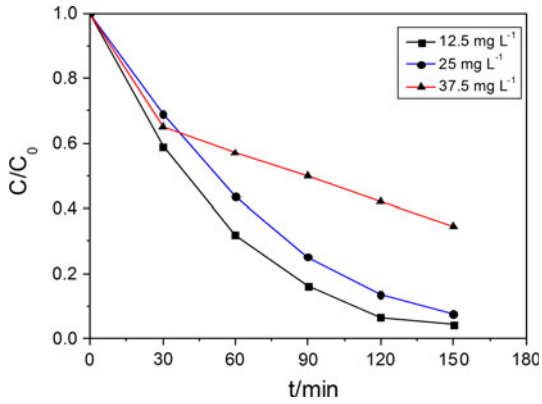

Fig. 11 Effect of initial concentration of MB on the degradation of MB over ⟨1.0% La-doped TiO_2⟩/$CoFe_2O_4$ nanofibers calcined at 600 °C

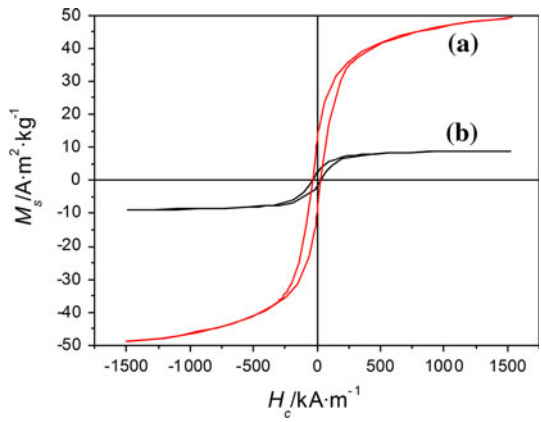

Fig. 12 Magnetic properties of $CoFe_2O_4$ nanofiber (*a*) and ⟨1.0% La-doped TiO_2⟩/$CoFe_2O_4$ nanofibers (*b*) in the applied field at room temperature

Acknowledgements This study was partly supported by the Natural Science Foundation of China (grant no. 51073005), the Beijing Natural Science Foundation (grant no. 2112013, KZ201010012012), PHR (IHLB), and the 973 Project (grant no. 2010CB933501).

References

1. Macwan DP, Dave PN, Chaturvedi S (2011) J Mater Sci 46:3669. doi:10.1007/s10853-011-5378-y
2. Zabova H, Cirkva V (2009) J Chem Techonl Biotechnol 84:1624. doi:10.1002/jctb.2220

3. Zhao JC, Chen CC, Ma WH (2005) Top Catal 35:269. doi:10.1007/s11244-005-3834-0
4. Dong WY, Lee CW, Luc XX, Sun YJ, Hua WM, Zhuang GS, Zhang SC, Chen JM, Hou HQ, Zhao DY (2010) Appl Catal B 95:197. doi:10.1016/j.apcatb.2009.12.025
5. Tacchini I, Terrado E, Ansón A, Martínez MT (2011) J Mater Sci 46:2097. doi:10.1007/s10853-010-5044-9
6. Ranjit KT, Cohen H, Willner I, Bossmann S, Braun AM (1999) J Mater Sci 34:5273. doi:10.1023/A:1004780401030
7. Kitsiou V, Filippidis N, Mantzavinos D, Poulios I (2009) Appl Catal B 86:27. doi:10.1016/j.apcatb.2008.07.018
8. Cao GX, Li YG, Zhang QH, Wang HZ (2010) J Am Ceram Soc 93:1. doi:10.1111/j.1551-2916.2009.03552.x
9. Chen JY, Qian YX, Wei XZ (2010) J Mater Sci 45:6018. doi:10.1007/s10853-010-4685-z
10. Chatterjee D, Mahata A (2001) Catal Commun 2:1. doi:10.1016/S1566-7367(00)00011-X
11. Usseglio S, Damin A, Scarano D, Bordiga S, Zecchina A, Lamberti C (2007) J Am Chem Soc 129:2822. doi:10.1021/ja066083m
12. Wang P, Zakeeruddin SM, Moser JE, Nazeeruddin MK, Sekiguchi T, Gratael M (2003) Nat Mater 2:402. doi:10.1038/nmat904
13. Zhu JF, Chen F, Zhang JL, Chen HJ, Anpo M (2006) J Photochem Photobiol A 180:196. doi:10.1016/j.jphotochem.2005.10.017
14. Ambrus Z, Balazs N, Alapi T, Wittmann G, Sipos P, Dombi A, Mogyorósi K (2008) Appl Catal B 81:27. doi:10.1016/j.apcatb.2007.11.041
15. Ranjit KT, Willner I, Bossmann SH, Braun AM (2001) Environ Sci Technol 35:1544. doi:10.1021/es001613e
16. Shao GS, Ma TY, Zhang XJ, Ren TZ, Yuan ZY (2009) J Mater Sci 44:6754. doi:10.1007/s10853-009-3628-z
17. Yu CL, Zhou WQ, Yang K, Rong G (2010) J Mater Sci 45:5756. doi:10.1007/s10853-010-4646-6
18. Kim H, Choi Y, Kanuka N, Kinoshita H, Nishiyama T, Usami T (2009) Appl Catal A 352:265. doi:10.1016/j.apcata.2008.10.016
19. Yogi C, Kojima K, Takai T, Wada N (2009) J Mater Sci 44:821. doi:10.1007/s10853-008-3151-7
20. Koepke C, Wisniewski K, Sikorski L, Piatkowski D, Kowalska K, Naftaly M (2006) Opt Mater 28:129. doi:10.1016/j.optmat.2004.10.034
21. Peng TY, Zhao D, Song HB, Yan CH (2005) J Mol Catal A: Chem 238:119. doi:10.1016/j.molcata.2005.04.066
22. Zhang YH, Zhang HX, Xu YX, Wang YG (2003) J Mater Chem 13:2261. doi:10.1039/B305538H
23. Jing LQ, Sun XJ, Xin BF, Wang BQ, Cai WM, Fu HG (2004) J Solid Chem 177:3375. doi:10.1016/j.jssc.2004.05.064
24. Li CJ, Wang JN, Li XY, Zhang LL (2011) J Mater Sci 46:2058. doi:10.1007/s10853-010-5038-7
25. Santala E, Kemell M, Leskela M, Ritala M (2009) Nanotechnology 20:1. doi:10.1088/0957-4484/20/3/035602
26. Zhang BF, Li CJ, Chang M (2009) Polym J 41:252. doi:10.1295/polymj.PJ2008270
27. Chiou CH, Wu CY, Juang RS (2008) Chem Eng J 139:322. doi:10.1016/j.cej.2007.08.002
28. Gennari FC, Pasquevich DM (1999) J Am Ceram Soc 82:1915. doi:10.1111/j.1151-2916.1999.tb02016.x
29. Porkodi K, Arokiamary SD (2007) Mater Charact 58:495. doi:10.1016/j.matchar.2006.04.019
30. Bacsa RR, Kiwi J (1998) Appl Catal B 1:19. doi:10.1016/S0926-3373(97)00058-1
31. Hurum DC, Agrios AG, Gray KA, Rajh T, Thurnauer MC (2003) J Phys Chem B 107:4545. doi:10.1021/jp0273934
32. Li CJ, Wang JN (2010) Mater Lett 64:586. doi:10.1016/j.matlet.2009.12.009
33. Li W, Frenkel AI, Woicik JC, Ni C, Ismat Shah S (2005) Phys Rev B 72:155315. doi:10.1103/PhysRevB.72.155315
34. Xu AW, Gao Y, Liu HQ (2002) J Catal 207:151. doi:10.1006/jcat.2002.3539
35. Cao GX, Li YG, Zhang QH, Wang HZ (2010) J Am Ceram Soc 93:25. doi:10.1111/j.1551-2916.2009.03364.x
36. Gupta SM, Tripathi M (2011) Chinese Sci Bull 56:1639. doi:10.1007/s11434-011-4476-1
37. Xiao Q, Zhang J, Xiao C, Si ZC, Tan XK (2008) Sol Energy 82:706. doi:10.1016/j.solener.2008.02.006
38. Wang XJ, Yao SW, Li XB (2009) Chin J Chem 27:1317. doi:10.1002/cjoc.200990220